HAL open science

Magnetic-field-induced ferroelectric states in centrosymmetric R2BaCuO5 (R=Dy and Ho)

Premakumar Yanda, F Orlandi, P Manuel, Nassira Boudjada, J Rodriguez-Carvajal, A Sundaresan

To cite this version:

Premakumar Yanda, F Orlandi, P Manuel, Nassira Boudjada, J Rodriguez-Carvajal, et al.. Magnetic-field-induced ferroelectric states in centrosymmetric R2BaCuO5 (R=Dy and Ho). Physical Review B, 2021, 104 (14), pp.144401. 10.1103/physrevb.104.144401 . hal-04179648

HAL Id: hal-04179648

https://hal.science/hal-04179648v1

Submitted on 10 Aug 2023

HAL is a multi-disciplinary open access archive for the deposit and dissemination of scientific research documents, whether they are published or not. The documents may come from teaching and research institutions in France or abroad, or from public or private research centers.

L'archive ouverte pluridisciplinaire **HAL**, est destinée au dépôt et à la diffusion de documents scientifiques de niveau recherche, publiés ou non, émanant des établissements d'enseignement et de recherche français ou étrangers, des laboratoires publics ou privés.

Magnetic-field-induced ferroelectric states in centrosymmetric R_2BaCuO_5 (R = Dy and Ho)

Premakumar Yanda,[1] F. Orlandi,[2] P. Manuel,[2] N. Boudjada,[3] J. Rodriguez-Carvajal,[4] and A. Sundaresan[1,*]

[1]*School of Advanced Materials, and Chemistry and Physics of Materials Unit, Jawaharlal Nehru Centre for Advanced Scientific Research, Jakkur 560064, India*

[2]*ISIS Facility, Rutherford Appleton Laboratory, Harwell Campus, Didcot OX11 0QX, United Kingdom*

[3]*Université Grenoble Alpes, Centre national de la recherche scientifique (CNRS), Institut Néel, 38000 Grenoble, France*

[4]*Institut Laue Langevin, Diffraction Group, CS 20156, 38042 Grenoble CEDEX 9, France*

(Received 13 March 2021; revised 18 September 2021; accepted 20 September 2021; published 1 October 2021)

The linear magnetoelectric effect and multiferroicity phenomena occur independently due to breaking inversion symmetry below the magnetically ordered state of either transition metal or rare-earth ions. Here, we report the occurrence of a linear magnetoelectric effect and magnetic field-induced ferromagnetism and ferroelectricity below T_N^R in the orthorhombic green phases R_2BaCuO_5 (R = Dy and Ho). They undergo a long-range antiferromagnetic ordering of Cu^{2+} (T_N^{Cu} = 18.5 and 17.5 K) and R^{3+} ions (T_N^{Dy} = 10.7 K and T_N^{Ho} = 8 K). The neutron diffraction study reveals that these compounds undergo a first-order magnetic transition from the high-temperature centrosymmetric antiferromagnetic phase (P_b112_1/n) to the low-temperature noncentrosymmetric phases $Pnm'a$ (Dy) and $P112_1'/a$ (Ho), which allow linear magnetoelectric coupling. This is consistent with field-induced electric polarization, below T_N^R, which varies linearly up to ~1.2 T. Above a critical field ($H_c > 1.2$ T), both compounds exhibit metamagnetic transitions with magnetization close to the saturation value $M_s \sim 10.1\ \mu_B$/f.u. (Dy) and ~11.8 μ_B/f.u. (Ho) at 7 T. Above the metamagnetic transition, a new polar state appears with large electric polarization, indicating field-induced ferroelectricity. We discuss the important role of $4f$-$3d$ coupling in determining the ground state magnetic structure responsible for the magnetoelectric coupling in both compounds.

DOI: 10.1103/PhysRevB.104.144401

I. INTRODUCTION

The magnetic interaction between $4f$ and $3d$ electrons has been a key research topic in condensed matter physics. It plays a pivotal role in deciding the properties of materials, such as magnetoresistance, superconductivity, magnetoelectricity, and most importantly, a wide variety of magnetic orderings. It is known that the interplay of $4f$ and $3d$ electrons of rare-earth (R) and transition metals (TMs), respectively, plays a crucial role in the magnetic properties and associated magnetoelectric coupling [1–5]. Furthermore, research on linear magnetoelectric and multiferroic materials has been a subject of interest because of the fundamental physics of strong coupling between spin and lattice degrees of freedom and their application potential, such as nonvolatile magnetoelectric memory, spintronic devices, etc. [1,6–12]. Such a cross-coupling in materials started with the theoretical and experimental observation of linear magnetoelectric effect in Cr_2O_3 [13,14]. In linear magnetoelectric materials, the induced electric polarization (magnetization) linearly increases with the applied magnetic field H (electric field E), which can be expressed as $P = \alpha H$ ($M = \alpha E$), where α denotes the magnetoelectric coupling coefficient [7,12,15]. Later, this field evolved into multiferroics where spontaneous magnetization and electric polarization coexist with a varying degree of coupling, depending on the origin of ferroelectricity [1,2,16,17]. Several materials have been reported to be linear magnetoelectric where TM or R ions are solely responsible for the magnetoelectricity [18–27]. However, only a few materials are known to exhibit the linear magnetoelectric effect or ferroelectricity resulting from the $4f$-$3d$ coupling [3,28,29].

The R_2BaCuO_5 family of compounds, where R = Sm-Lu and Y, so-called *green phases*, exhibit various magnetic structures depending on the R ion due to $4f$-$3d$ exchange interaction and R ion magnetic anisotropy [4,30–38]. The ground state magnetic structures possess different propagation vectors for each compound, for example, $\mathbf{k}_C = (0, 0, 0)$ for R = Sm, Dy; $\mathbf{k}_{C1} = (0, \frac{1}{2}, 0) + \mathbf{k}_{C2} = (0, 0, 0)$ for Ho; $\mathbf{k}_C = (0, \frac{1}{2}, \frac{1}{2})$ for R = Y; $\mathbf{k}_C = (0, \frac{1}{2}, 0)$ for R = Er and Tm; and $\boldsymbol{k}_C = (0, 0, \frac{1}{2})$ for R = Gd [4,38–41]. In the viewpoint of magnetic symmetry analysis, these compounds might be promising candidates to exhibit either magnetoelectric or multiferroic properties [42]. Recently, a linear magnetoelectric effect has been reported below $T_N^{Cu} = 23$ K in Sm_2BaCuO_5 [38]. Below the independent ordering of Sm ($T_N^{Sm} = 5$ K), the electric polarization decreases. The scenario is completely different in Gd_2BaCuO_5, where both copper and Gd moments order at the same temperature ($T_N = 11.8$ K). It exhibits an incommensurate magnetic structure (elliptical interpenetrated cycloids) possessing a modulation vector $\mathbf{k} = (0, 0, g)$, with $g = 0.4446$ below $T_N = 11.8$ K, and undergoes lock-in transition at $T_{loc} = 6$ K to a commensurate structure with

*sundaresan@jncasr.ac.in

 ©2021 American Physical Society

$\mathbf{k}_C = (0, 0, \frac{1}{2})$ [4]. Moreover, this compound shows spontaneous electric polarization at the magnetic ordering temperature. Dy_2BaCuO_5 exhibits a magnetoelectric effect, but the microscopic mechanism responsible for magnetoelectric coupling is unknown [37]. On the other hand, there are no reports on the electrical properties of Ho_2BaCuO_5, to the best of our knowledge.

Here, we report the observation of a linear magnetoelectric effect, magnetic field-induced ferromagnetism, and ferroelectricity in the compounds R_2BaCuO_5 (R = Dy and Ho). These isostructural compounds crystallize in the centrosymmetric orthorhombic structure (*Pnma*), containing an unusual distorted CuO_5 square pyramid. Dy_2BaCuO_5 and Ho_2BaCuO_5 show long-range antiferromagnetic ordering of copper ions at 18.5 and 17.5 K, and Dy^{3+} and Ho^{3+} moments order at 10.7 and 8 K, respectively. The applied magnetic field induces electric polarization at the Dy^{3+}/Ho^{3+} ordering temperatures. Both compounds exhibit metamagnetic transitions above a critical field with a large magnetization and electric polarization. Our results demonstrate that the R_2BaCuO_5 (R = Dy and Ho) compounds represent magnetoelectric materials where the $4f$-$3d$ interactions play a crucial role.

II. EXPERIMENT

Polycrystalline samples of R_2BaCuO_5 (R = Dy and Ho) were prepared by heating a stoichiometric mixture of high-purity R_2O_3 (preheated), $BaCO_3$, and CuO at 950 °C in air. The elemental composition was probed with energy dispersed x-ray analysis (EDS) equipped with ZEISS GEMINI 500 FESEM. X-ray powder diffraction patterns were recorded using a PANalytical Empyrean diffractometer with Cu Kα1 radiation. Neutron diffraction measurements on Dy_2BaCuO_5 were carried out on the WISH instrument at ISIS [43]. Two different samples of Ho_2BaCuO_5 have been used in this paper; the sample used on D1B, ILL was free of impurities and was synthesized and measured a long time ago (1993) using thermal scans between 2 and 32 K. Another sample containing $< 1\%$ of cubic Ho_2O_3 was measured on the WISH instrument, ISIS. Magnetization measurements were performed by a superconducting quantum interference device magnetometer (MPMS, Quantum Design). The specific heat (C_p) was measured in a physical property measurement system (PPMS, Quantum design). To measure the dielectric and pyrocurrent (electric polarization), the silver paste was applied on both sides of the sample pellet while a PPMS provided the temperature and magnetic field control. The dimensions of the pellets were $t = 0.279$ mm and $A = 20\,\text{mm}^2$ for Dy_2BaCuO_5 and $t = 0.33$ mm and $A = 50\,\text{mm}^2$ for Ho_2BaCuO_5. The dielectric constant as a function of temperature under different magnetic fields was recorded using an Agilent E4980A LCR meter. Before pyroelectric current measurement, the sample was subjected to magnetoelectric poling, where an electric field and magnetic field were applied while cooling across T_N and then short-circuited for 15 min to remove stray charges. The temperature dependence of pyrocurrent was measured with a Keithley 6517A electrometer, and electric polarization was obtained by integrating the pyrocurrent with respect to time.

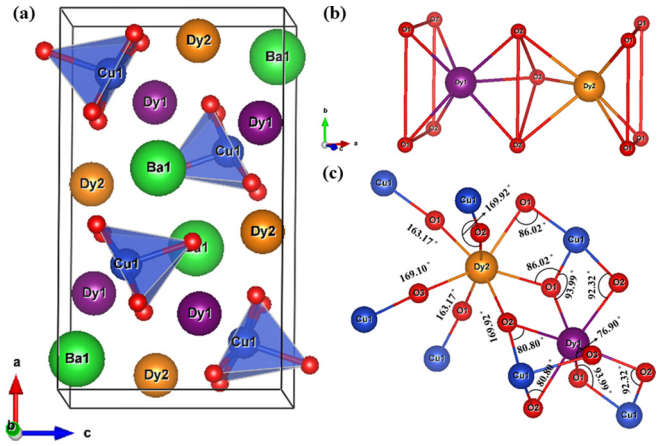

FIG. 1. (a) Crystal structure of Dy_2BaCuO_5 at 25 K. (b) Dy_2O_{11} blocks are formed by triangular face-shared DyO_7 polyhedrons. (c) Inequivalent Dy sites with Dy-O-Cu bond angles.

III. RESULTS AND DISCUSSIONS

The results of EDS analysis, as shown in Figs. S1 and S2 in the Supplemental Material [44], reveal the stoichiometric composition of both compounds. Rietveld refinement of room temperature x-ray diffraction data (see Figs. S3 and S4 in the Supplemental Material [44]) confirmed that R_2BaCuO_5 (R = Dy and Ho) crystallize in orthorhombic nonpolar structure (space group: *Pnma*). The corresponding structural parameters are provided in Tables SI and SII in the Supplemental Material [44]. To check whether these compounds undergo any structural phase transition, we carried out neutron diffraction at low temperatures. A careful analysis of these data (see Figs. S5 and S6 in the Supplemental Material [44]) confirmed that the centrosymmetric crystal structure (*Pnma*1′) is stable down to the lowest temperature measured in the paramagnetic state. The crystal structure and structural parameters obtained from the refinement of neutron data (WISH) of Dy_2BaCuO_5 at 25 K are shown in Fig. 1 and Table I, respectively. For the Ho_2BaCuO_5 compound, the structural data obtained from neutron data (WISH) refinement at 20 K are provided in Table II. The crystal structure (except the change of cell parameters with temperature) is quite close to the room temperature data published earlier [45]. The crystal structure of Dy_2BaCuO_5 given in Fig. 1 is equally valid for R_2BaCuO_5

TABLE I. Structural parameters of Dy_2BaCuO_5 obtained from Rietveld refinement of neutron data collected at 25 K. Space group: *Pnma*1′; $a = 12.2025(2)$ Å, $b = 5.6733(1)$ Å, $c = 7.1379(1)$ Å, Vol: 494.14 (1) Å^3; global $\chi^2 = 5.64$; Rp = 1.90, wRp = 2.25.

Atom	Site	x	y	z	B_{iso}(Å^2)
Dy1	4c	0.2889 (1)	0.2500	0.1172 (1)	0.047 (8)
Dy2	4c	0.0743 (1)	0.2500	0.3968 (1)	0.047 (8)
Ba	4c	0.9075 (2)	0.2500	0.9288 (3)	0.230 (5)
Cu	4c	0.6600 (1)	0.2500	0.7115 (2)	0.790 (1)
O1	8d	0.4332 (2)	−0.0082 (2)	0.1686 (2)	0.490 (2)
O2	8d	0.2282 (1)	0.5057 (3)	0.3552 (3)	0.490 (2)
O3	4c	0.1005 (2)	0.2500	0.0837 (3)	0.490 (2)

TABLE II. Structural parameters of Ho_2BaCuO_5 obtained from Rietveld refinement of neutron TOF data collected at 20 K using the two highest resolution banks ($2\theta = 152^\circ$ and 121°). Space group: *Pnma*1′; $a = 12.1668(5)$ Å, $b = 5.6553(2)$ Å, $c = 7.1135(3)$ Å, Vol: 489.46 (4) Å^3; global $\chi^2 = 9.99$; Bragg R-factor: (152 °) = 2.32; (121 °) = 3.11.

Atom	Site	x	y	z	B_{iso}(Å^2)
Ho1	4c	0. 2880 (1)	0.2500	0.1152 (2)	0.34 (4)
Ho2	4c	0.0740 (1)	0.2500	0.3952 (2)	0.50 (4)
Cu	4c	0.6601 (1)	0.2500	0.7110 (2)	0.77 (4)
Ba	4c	0.9057 (2)	0.2500	0.9286 (3)	0.34 (5)
O1	8d	0.4324 (1)	−0.0076 (3)	0.1670 (1)	0.93 (4)
O2	8d	0.2278 (1)	0.5061 (3)	0.3557 (2)	0.85 (4)
O3	4c	0.1011 (2)	0.250	0.0811 (3)	0.79 (5)

(R = Sm-Lu and Y). The structure consists of monocapped trigonal prisms RO_7 connected by trigonal faces to form R_2O_{11} blocks, whose cavities are occupied by Cu^{2+} and Ba^{2+} ions. The Cu^{2+} ions are in isolated square pyramids CuO_5 and Ba^{2+} ions found in BaO_{11} polyhedrons. It is important to note that all the cations occupy the fourfold sites (Wyckoff position 4c in *Pnma*) with mirror symmetry, and there are two inequivalent sites for rare earth R^{3+} ions, as shown in Fig. 1(b). The oxygen coordination polyhedrons of R^{3+} in both sites differ slightly, but the local environment varies significantly. The R^{3+} ions at the $R2$ site are connected through oxygen atoms to six Cu^{2+} ions, and five of six $R2$-O-Cu bond angles are ∼180 °, while the R^{3+} ions in the $R1$ site are connected only to three Cu^{2+} ions with $R1$-O-Cu bond angles ∼90 °, as shown in Fig. 1(c).

Based on synchrotron and pyrocurrent measurements, it has been reported that Dy_2BaCuO_5 exhibits a nonpolar (*Pnma*)-to-polar ($Pna2_1$) transition at 232 K [37]. However, as discussed earlier, our neutron diffraction experiments revealed that the nonpolar *Pnma* structure is stable down to the lowest temperature measured. Further, our heat capacity measurements did not show any evidence for structural phase transition in this compound, as shown in Fig. S7 in the Supplemental Material [44]. Moreover, our pyrocurrent measurements showed a monotonous increase of current without any anomaly (see Fig. S7 in the Supplemental Material [44]). We believe that the pyrocurrent anomaly reported earlier at high temperature might be due to thermally stimulated free charge carriers which are of extrinsic origin and sample dependent [37,46]. Also, the absence of hysteresis in PE loop measurements at 77 K for both compounds (Fig. S8 in the Supplemental Material [44]) is consistent with the centrosymmetric crystal structure.

The temperature dependence of magnetization of R_2BaCuO_5 (R = Dy and Ho), measured under different magnetic fields, and specific heat measured under zero magnetic field are displayed in Fig. 2. As seen in Fig 2(a), Dy_2BaCuO_5 exhibits long-range magnetic ordering of Cu^{2+} and Dy^{3+} moments at $T_N^{Cu} = 18.5$ K and $T_N^{Dy} = 10.7$ K, respectively. At the same time, the Ho compound exhibits long-range magnetic ordering at $T_N^{Cu} = 17.5$ K and $T_N^{Ho} = 8$ K, as seen in Fig. 2(d). In DC magnetization, we do not observe any anomaly at T_N^{Cu} due to the high paramagnetic moment of Dy^{3+} and Ho^{3+} ions. The possible magnetic interaction path in these compounds is Cu^{2+}-O^{2-}-Dy^{3+}-O^{2-}-Cu^{2+} because each copper ion is isolated, and there are no Cu-O-Cu bonds. The effective magnetic moment is in good agreement with the theoretical value of the R^{3+} and Cu^{2+} ions (Fig. S9 in the Supplemental Material [44]). The negative sign of the Curie-Weiss constant indicates the dominating antiferromagnetic interactions in these compounds. Upon increasing the applied magnetic field, the anomaly at $T_N^{Dy} = 10.7$ K and $T_N^{Ho} = 8$ K in DC magnetization (M/H vs T) is suppressed, indicating possible metamagnetic transitions or changes in magnetic structure [Figs. 2(b) and 2(e)]. Indeed, below T_N^R, the isothermal $M(H)$ curves exhibit field-induced steps, which is the signature of the metamagnetic nature of the phase transitions, as shown in Figs. 2(c) and 2(f). This behavior can be seen from the dM/dH curves, given in insets of Figs. 2(c) and 2(f) and S10 in the Supplemental Material [44]. These data show an initial linear behavior below a critical field ($H_c \sim 1.2$ T) due to the antiferromagnetic ordering. Above the critical field, both compounds show field-induced metamagnetic transitions leading to large magnetization with values up to ∼10.1 μ_B/f.u. (Dy) and ∼11.8 μ_B/f.u. (Ho) at 7 T and 2 K. Upon increasing the temperature, the metamagnetic transitions shift to lower fields.

To check the possibility of linear magnetoelectric effect, we have performed the electrical measurements on both compounds in $E \perp H$ and $E \parallel H$ configurations [47]. Figures 3(a) and 3(b) show the temperature-dependent dielectric constant at different magnetic fields for Dy_2BaCuO_5 and the corresponding dissipation factor measured under $E \perp H$ configuration. An apparent dielectric anomaly is seen at T_N^{Dy} under zero magnetic field, but there is no noticeable feature at copper ordering temperature. With increasing magnetic fields, the dielectric anomaly develops into a peaklike feature. In addition, a small dielectric peak appears ∼4.5 K above the magnetic field of 2 T, which is suppressed >3 T. A notable magnetodielectric (MD) effect is observed around T_N^{Dy} with the value of 0.16%, as can be seen in Fig. S11 in the Supplemental Material [44]. Moreover, MD curves also show signatures of metamagnetic transitions under magnetic fields. The appearance of the dielectric peak at the Dy magnetic ordering indicates a possible ferroelectric transition. To check this, we have recorded the pyroelectric current as a function of temperature and magnetic field after magnetoelectric poling in $E \perp H$ configuration, which is shown in Fig. 3(c). We have not observed the pyrocurrent anomaly under a zero magnetic field. However, a clear asymmetric pyrocurrent peak appears at T_N^{Dy} under applied magnetic fields. At magnetic fields >1.2 T, the pyrocurrent peaks continue to be present. However, the pyrocurrent peaks start decreasing with further increasing of the field. In addition to this, we have observed another pyrocurrent peak at 4.5 K between 2 and 3 T, as observed in dielectric data, indicating another field-induced change in magnetic structure.

The corresponding electric polarization is shown in Fig. 3(d). Unlike Sm_2BaCuO_5, where the polarization appears at the copper ordering temperature, Dy_2BaCuO_5 shows the polarization at dysprosium ordering T_N^{Dy} under magnetic field

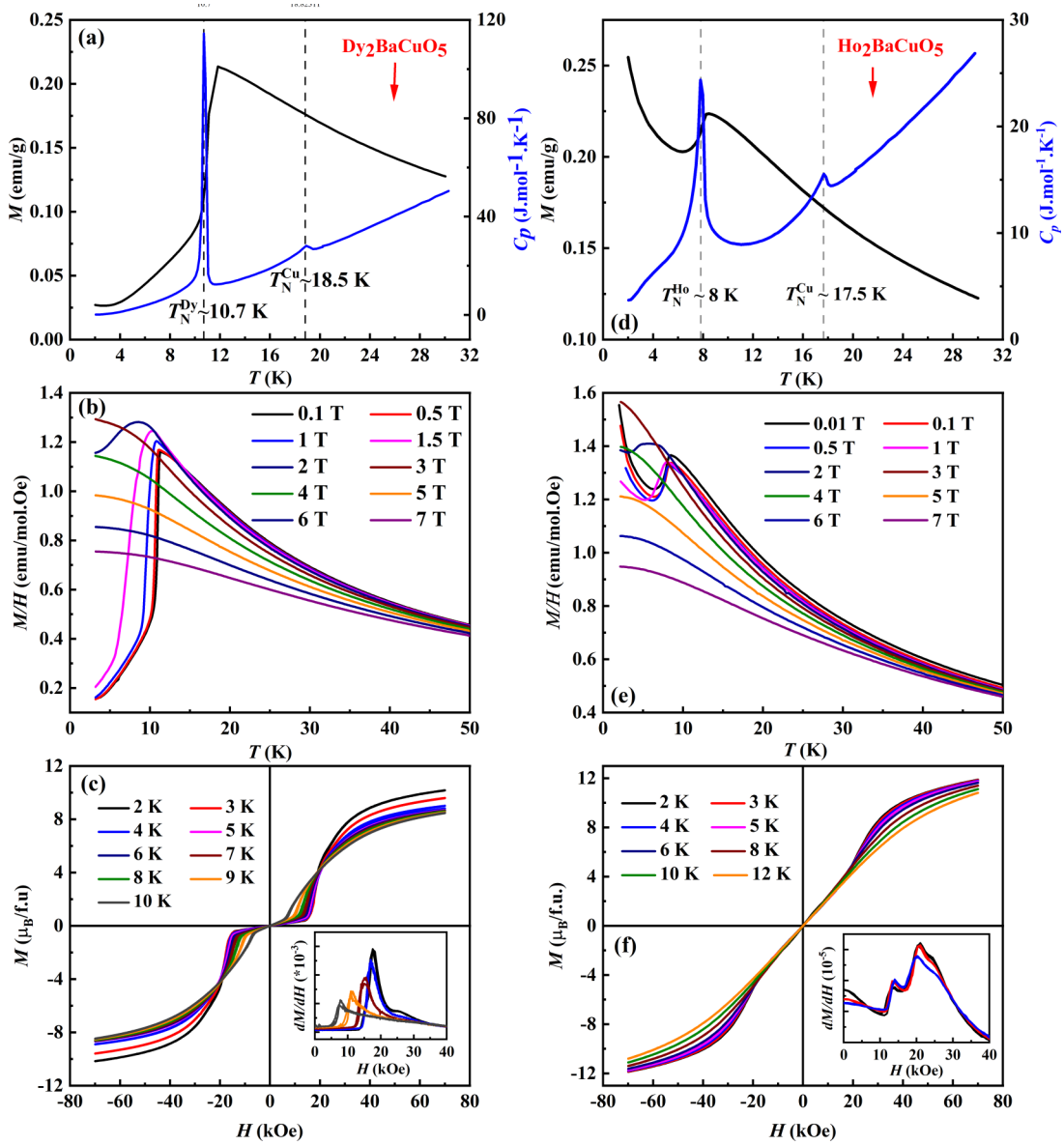

FIG. 2. (a) and (d) Left axis: Temperature-dependent DC magnetization measured under 100 Oe in field-cooled (FC) condition. Right axis: Specific heat measured under zero magnetic field. (b) and (e) DC magnetization measured under different magnetic fields. (c) and (f) Isothermal $M(H)$ curves for Dy_2BaCuO_5 and Ho_2BaCuO_5, respectively. Insets show dM/dH vs H.

[38]. With increasing magnetic field, electric polarization increases linearly up to metamagnetic transition, as shown in Fig. S12(a) in the Supplemental Material [44], demonstrating the linear magnetoelectric effect. Above the metamagnetic transition, electric polarization becomes nonlinear and finally suppressed at high fields, as seen from the inset of Fig. 3(d). The nonlinear behavior indicates the symmetry of the new magnetic phase above the metamagnetic transition might be polar. Similar linear magnetoelectric effect and field-induced magnetoelectric coupling are reported in $DyCrO_4$, where the presence of polar symmetry above the metamagnetic transition is confirmed by neutron diffraction [29]. As indicated by the pyrocurrent peak, there is an additional polarization between 2 and 3 T at 4.5 K [see Figs. 3(c) and 3(d)]. However, one must perform single-crystal neutron diffraction experiments under magnetic fields to understand the nature of the field-induced magnetic structures. The maximum polarization observed is $\sim 14.6\,\mu C/m^2$ at magnetic field $H = 2.5$ T and 2 K. The intrinsic nature of the linear magnetoelectric effect and field-induced ferroelectric transitions is further supported by switching polarization and DC bias measurements, as depicted in Figs. 3(e) and 3(f). The calculated magnetoelectric coefficient α of Dy_2BaCuO_5 is 3.47 ps/m (1 T and 10 K) and 7.37 ps/m (2.5 T and 2 K), which is higher than that of the isostructural compound Sm_2BaCuO_5 [38].

The outcome of the electrical measurements measured in the $E \perp H$ configuration for Ho_2BaCuO_5 is provided in Fig. 4. Unlike the Dy_2BaCuO_5, this compound exhibits multiple metamagnetic transitions and associated dielectric properties under applied magnetic fields. The temperature-dependent dielectric constant and the corresponding dissipation factor for Ho_2BaCuO_5 are shown in Figs. 4(a) and 4(b). It is

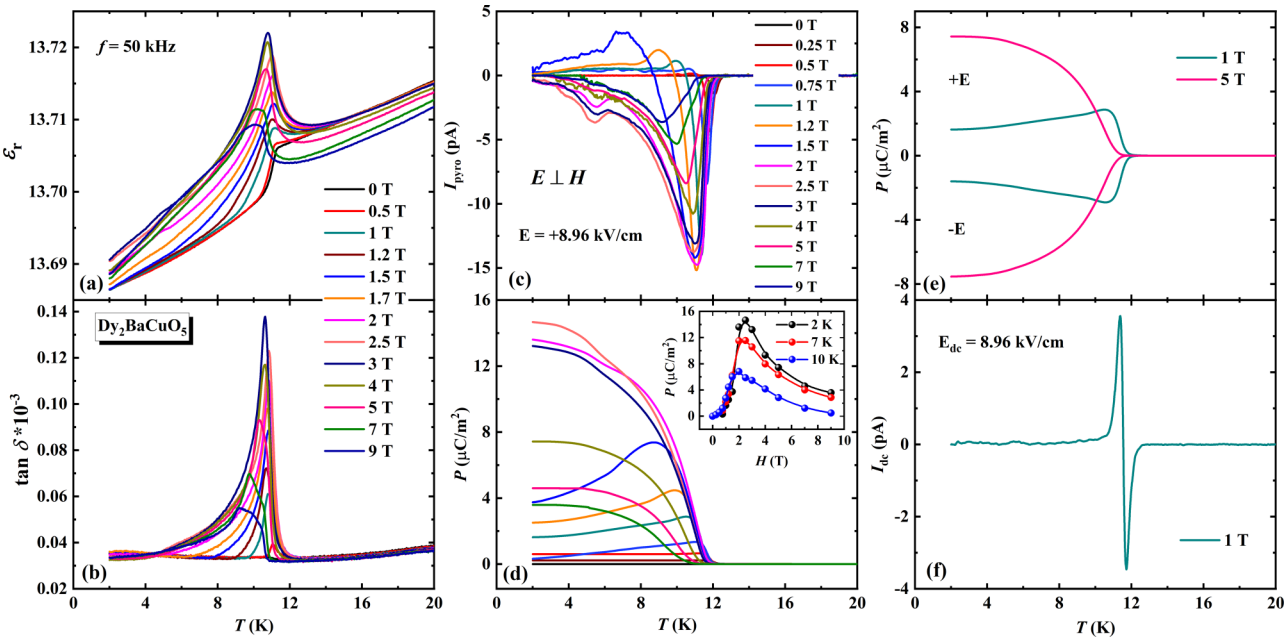

FIG. 3. (a) and (b) Temperature-dependent dielectric constant and corresponding loss measured under different magnetic fields and frequency $f = 50$ kHz, respectively. (c) T dependence of pyrocurrent recorded for different magnetic fields with the poling electric field $E = +8.96$ kV/cm. (d) Polarization is obtained by integrating the pyrocurrent with respect to time. The inset shows magnetic field-dependent polarization. (e) Switching of polarization by changing the direction of the poling electric field measured under 1 and 5 T magnetic fields. (f) Direct current (DC) bias at 1 T, measured in $E \perp H$ for Dy_2BaCuO_5.

evident from the figure that there is an anomaly at T_N^{Ho} in the absence of a magnetic field. The anomaly increases under applied magnetic fields and finally disappears at >3 T. Interestingly, there is a second dielectric anomaly below T_N^{Ho} at 1 T, which shifts to low temperatures with further increasing of the magnetic field. In addition, there are new anomalies at high fields ($H > 5$ T) at very low temperatures. The temperature-dependent pyrocurrent measured at selected magnetic fields and the corresponding electric polarization are shown in Figs. 4(c) and 4(d). No polarization is observed at $H = 0$ T at temperatures down to 2 K. However, the external magnetic field induces an electric polarization, at T_N^{Ho}, that varies linearly up to 1 T, as seen from Fig. S12(b) in the Supplemental Material [44] and inset of Fig. 4(d), demonstrating the linear magnetoelectric effect. In addition, it is clear from the pyrocurrent data [see Fig. 4(c)] that there is a broad anomaly ~4 K under the magnetic field. At $H \geqslant 1$ T, pyrocurrent anomalies near T_N^{Ho} show two peak features indicating that the second dielectric anomaly is associated with ferroelectricity. This second transition can be related to the metamagnetic transition. A maximum polarization of 32.9 μC/m^2 is observed at 2 K and 1 T. The calculated magnetoelectric coefficient α of Ho_2BaCuO_5 at 5 K is 41.4 ps/m for ~1 T, higher than that of the isostructural compounds Sm_2BaCuO_5, Dy_2BaCuO_5, and most of the known magnetoelectrics. Further, DC bias measurement and switching nature of electric polarization, as seen from Figs. 4(e) and 4(f), confirm the intrinsic nature of electric polarization and demonstrate the two transitions discussed above. The results obtained under $E \parallel H$ configuration for Dy_2BaCuO_5 and Ho_2BaCuO_5 are shown in Figs. S13 and S14 in the Supplemental Material [44], respectively. The observed electric polarization in $E \perp H$ configuration is higher than that of $E \parallel H$ configuration, indicating nonzero off-diagonal magnetoelectric tensors for both compounds [47].

The magnetic field dependence of magnetization, relative dielectric constant, magnetoelectric current, and electric polarization at 5 K for polycrystalline Ho_2BaCuO_5 are shown in Fig. 5. The derivative of the magnetization [Fig. 5(a)] shows an anomalous behavior that indicates field-induced metamagnetic transitions under applied magnetic fields. Similarly, the dielectric constant displays a corresponding anomalous behavior with the magnetic field, as seen from Fig. 5(b). The magnetoelectric current [Fig. 5(c)] was recorded from −1 to 9 T at 5 K, after poling the sample with 6.7 kV/cm and magnetic field of −1 T, and the corresponding polarization is given in Fig. 5(d). As shown in Fig. 5(d), there is no polarization at zero magnetic fields, and upon increasing the magnetic field, electric polarization appears with a linear increase up to ~1 T and reaches a maximum at ~1.3 T. With further increase of the magnetic field, polarization shows anomalous behavior and finally vanishes >7 T. These results demonstrate that Ho_2BaCuO_5 exhibits linear magnetoelectric effect and field-induced ferroelectric transitions.

To examine further the linear magnetoelectric effect in both compounds, we carried out magnetic field-dependent magnetoelectric current measurements in the linear magnetoelectric region (<1 T). In this measurement, we have poled the sample in the presence of an electric field and magnetic field (−1 T) across T_N^R to 2 and 5 K for Dy_2BaCuO_5 and Ho_2BaCuO_5, respectively. Subsequently, we have recorded the current in response to the sweeping of the magnetic field from −1 to +1 T at fixed temperatures, which are presented in Fig. 6. As seen from the figure, the magnetoelectric current changes periodically with the applied magnetic field. However, the

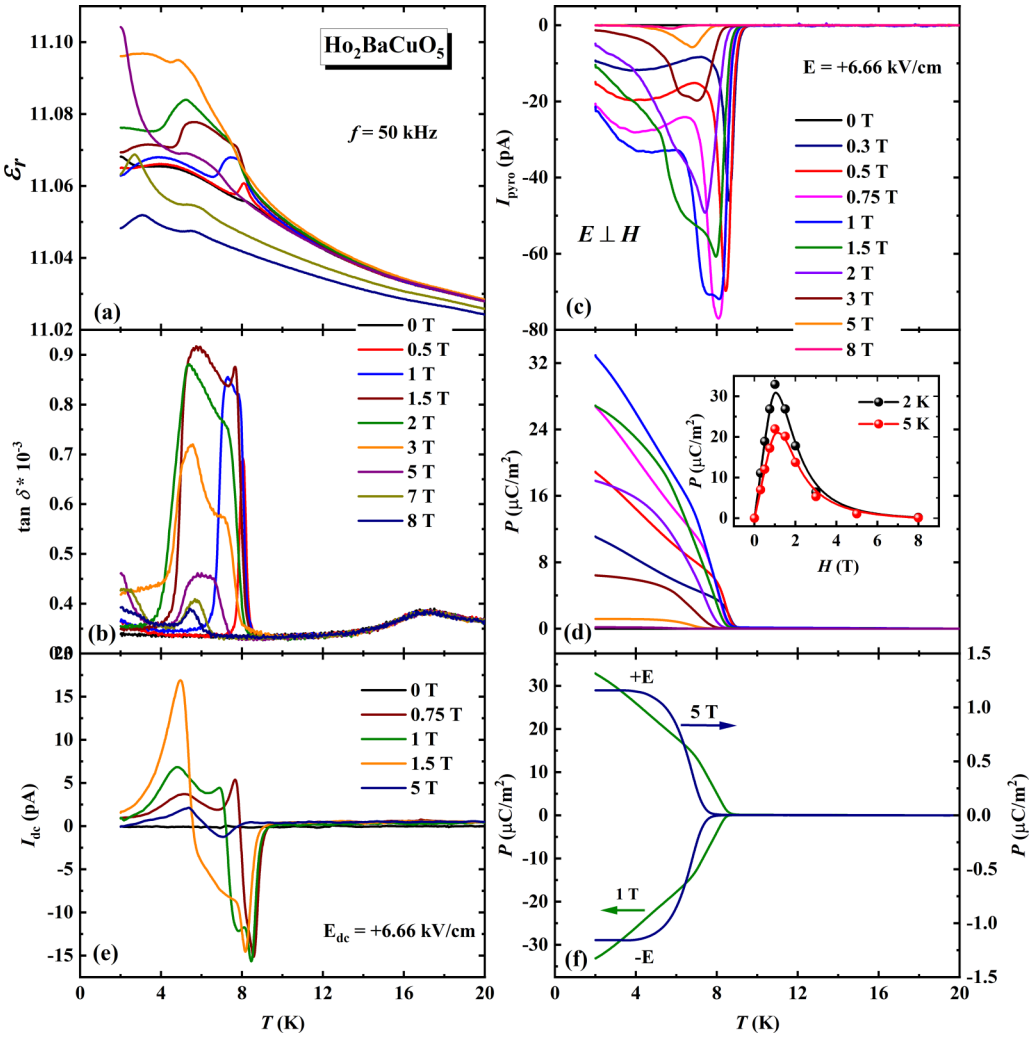

FIG. 4. (a) and (b) Dielectric constant against temperature measured with frequency $f = 50$ kHz under different magnetic fields and corresponding loss, respectively. (c) and (d) *T*-*H*-dependent pyrocurrent and electric polarization. (e) The obtained DC bias signal under different magnetic fields. (f) Switching of polarization at 1 and 5 T, for Ho_2BaCuO_5.

corresponding polarization oscillates linearly with the magnetic field, providing evidence of the linear magnetoelectric effect.

A. Magnetic structure of R_2BaCuO_5 (R = Dy and Ho)

We have carried out the neutron diffraction measurements below and above the magnetic ordering temperatures on both compounds to understand the observed linear magnetoelectric effect. From our neutron data (WISH) of Dy_2BaCuO_5, we obtained the **k**-vectors $(0, \frac{1}{2}, 0)$ at $T_N^{Dy} < T \leqslant T_N^{Cu}$ and $(0, 0, 0)$ at $T \leqslant T_N^{Dy}$ by using the k_SEARCH program in the FULLPROF SUITE [48]. Knowing the crystal structure ($Pnma1'$) and **k**-vector, we have used ISODISTORT to determine the possible magnetic modes and associated magnetic space groups [49]. We found six possible magnetic models, which correspond to two two-dimensional (2D) irreducible representations (*irreps*) with different order parameters. In the temperature interval $T_N^{Dy} < T \leqslant T_N^{Cu}$, the correct solution is found to be centrosymmetric with the magnetic space group symbol P_b112_1/n (transformation to standard-setting P_a2_1/c can be performed by **b**, **a**, −**b**-**c**; 0, 0, 0) which represents *irrep* mY1: (a, a) (see Fig. S15 in the Supplemental Material [44]). The equivalent Hall symbol [50] is $\bar{P}2_n1'_b$, in which the presence of a center of symmetry is explicit by the bar on top of the primitive lattice symbol. From the symmetry, it is evident that the corresponding point group $(2/m1')$ imposes a null magnetoelectric tensor consistent with the absence of the magnetoelectric effect. The obtained magnetic structure is commensurate but noncollinear, as illustrated in Fig. 7(a). We have fixed the z component of the Dy1 moment to zero because there are correlations between the z components of Dy1 and Cu in the refinement, resulting in high errors, and the Dy1 moment was close to zero. From Fig. 7(a), the Cu and Dy2 moments lie in the **ac**-plane, and Dy1 moments are pointed along the x axis. The moment of the Dy2 is considerably high compared with Dy1 on account of the higher molecular field on Dy2, which is surrounded by six Cu^{2+} ions, whereas Dy1 is surrounded by three Cu^{2+} ions. The Dy1 moments are aligned along the Dy1-O3 bond and this is not the case for Dy2. This different behavior is due to the different single-ion anisotropy of both sites.

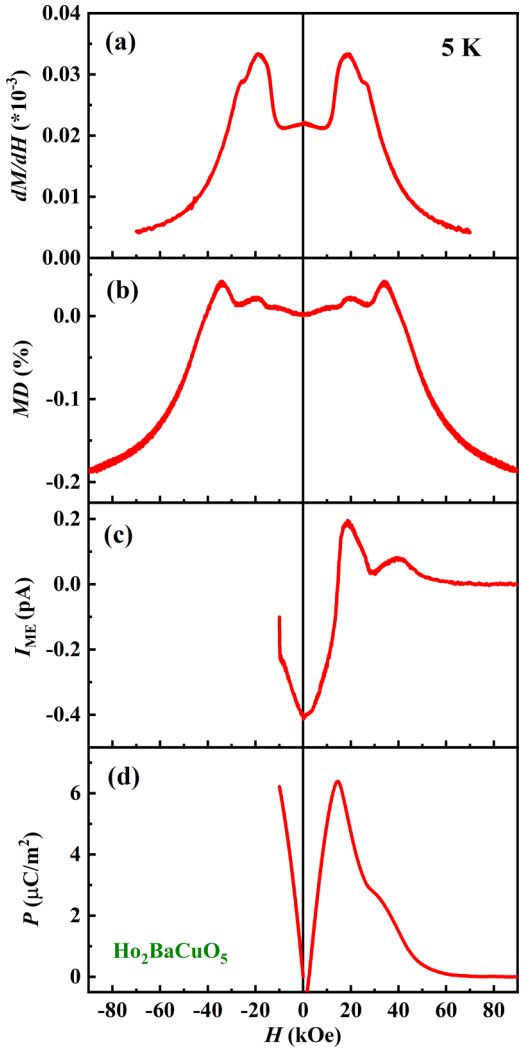

FIG. 5. Magnetic field dependent (a) derivative of magnetization obtained from M vs H curve at 2 K. (b) Relative dielectric constant measured at $f = 50$ kHz. (c) Magnetoelectric current recorded after poling the Ho_2BaCuO_5 sample under electric and magnetic fields. (d) Electric polarization is obtained by integrating the magnetoelectric current.

We have solved the ground state structure from the data (WISH) collected at 1.5 K (below $T < T_N^{Dy}$) with the $\mathbf{k} = (0, 0, 0)$. There are eight possible solutions corresponding to eight one-dimensional (1D) *irreps*, out of which the following four *irreps* mGM_1^- ($Pn'm'a'$), mGM_2^- ($Pnma'$), mGM_3^- ($Pn'ma$), and mGM_4^- ($Pnm'a$) allow the linear magnetoelectric effect. We have systematically tested all eight possible solutions, and the preferred solution is $Pnm'a$, which belongs to *irrep* mGM_4^- (see Fig. S16 in the Supplemental Material [44]). The corresponding magnetic structure is illustrated in Fig. 7(b). In this structure, Cu moments lie in the **ac**-plane, Dy1 and Dy2 moments are preferentially oriented along the **a** and **c** axes, respectively. There are small components of the magnetic moment along the **c** axis for Dy1 and along the **a** axis for Dy2. The moment projections with respect to temperature for all three magnetic cations Dy1, Dy2, and Cu are presented in Fig. 8. At T_N^{Cu}, there is an induced moment in Dy sublattices which indicates the importance of exchange paths of type Cu^{2+}-O^{2-}-Dy^{3+}-O^{2-}-Cu^{2+} and the strong $4f$-$3d$ coupling present in this compound. The deduced magnetic point group $mm'm$ allows the linear magnetoelectric effect.

The magnetic phase transitions in Ho_2BaCuO_5 are like those of the Dy_2BaCuO_5 compound. However, the ground state of the Ho compound conserves the two propagation vectors $\mathbf{k}_{C1} = (0, \frac{1}{2}, 0)$ and $\mathbf{k}_{C2} = (0, 0, 0)$, as it is seen in the diffraction patterns (see the upper panel of Fig. S17 in the Supplemental Material [44]). The first transition, on cooling, takes place at $T_N^{Cu} = 17.5$ K; like Dy_2BaCuO_5, the propagation vector is $\mathbf{k}_{C1} = (0, \frac{1}{2}, 0)$, and the magnetic space group is monoclinic P_b112_1/n, which is allowed by the *irrep* mY1 (a, a). From the symmetry, it is evident that the magnetic point group ($2/m1'$) imposes a null magnetoelectric tensor, which is consistent with our electrical measurements. The refined diffraction patterns at 8.3 K (D1B) and 12 K (WISH) are given in Fig. S18 in the Supplemental Material [44], and the results of these refinements are provided in Tables SIII and SIV in the Supplemental Material [44]. The magnetic structure obtained from the refinement at 12 K (WISH) and 8.3 K (D1B), displaying only magnetic atoms, are depicted in Figs. 9(a) and S19 in the Supplemental Material [44], respectively.

Below $T_N^{Ho} = 8$ K, the magnetic structure possesses two propagation vectors, namely, $\mathbf{k}_{C1} = (0, \frac{1}{2}, 0)$ and $\mathbf{k}_{C2} = (0, 0, 0)$, as can be seen from the bottom panel of Fig. S17 in the Supplemental Material [44]. The magnetic structure may be analyzed in two ways; one way is to consider two magnetic phases corresponding to the two propagation vectors and another with a single magnetic phase, which can be obtained by studying the isotropy subgroups associated with the mixture of *irreps* of the two propagation vectors. The refinement with two magnetic phases P_b112_1/n ($\mathbf{k}_{C1}$) and $Pnm'a$ ($\mathbf{k}_{C2}$) gives an excellent fit to the experimental data. The details of this refinement are provided in the Supplemental Material [44]. In the case of a single magnetic phase model, two possibilities (type-3 orthorhombic and monoclinic magnetic groups) are close to explaining the experimental results. The orthorhombic group $P2_1'm'n$ [standard setting $Pm'n2_1'$, No. 31.125, 1D-$\mathbf{k}_{C2}$ *irreps*: mGM_4^-, and 2D-$\mathbf{k}_{C1}$ *irreps*: mY_1: (a, 0)] gives a relatively good refinement of the D1B data at 2.3 K, as shown in Fig. S22 in the Supplemental Material [44]. Nevertheless, the fit is worse than that of the two magnetic phases case, and then it corresponds to a false minimum [44].

Whereas the refinement with monoclinic magnetic group $P112_1'/a$, which we discuss later, gives an excellent fit comparable with that of two magnetic phases refinement, thus making it difficult to distinguish between these two solutions, the temperature evolution of ($0\ \frac{1}{2}\ 0$) and ($0\ \frac{1}{2}\ 1$) reflections (see Fig. S20 in the Supplemental Material [44]) suggests that the single magnetic phase with the monoclinic magnetic structure is the plausible model. The reflection ($0\ \frac{1}{2}\ 0$) behaves like an induced moment and ($0\ \frac{1}{2}\ 1$) that relates primarily to Cu positions clearly shows a jump at T_N^{Ho}. In phase coexistence (two magnetic phases), such a different behavior between reflections belonging to the same propagation vector is unlikely. Therefore, the coherent superposition of the modes (single magnetic phase) with monoclinic $P112_1'/a$ is the correct solution [51].

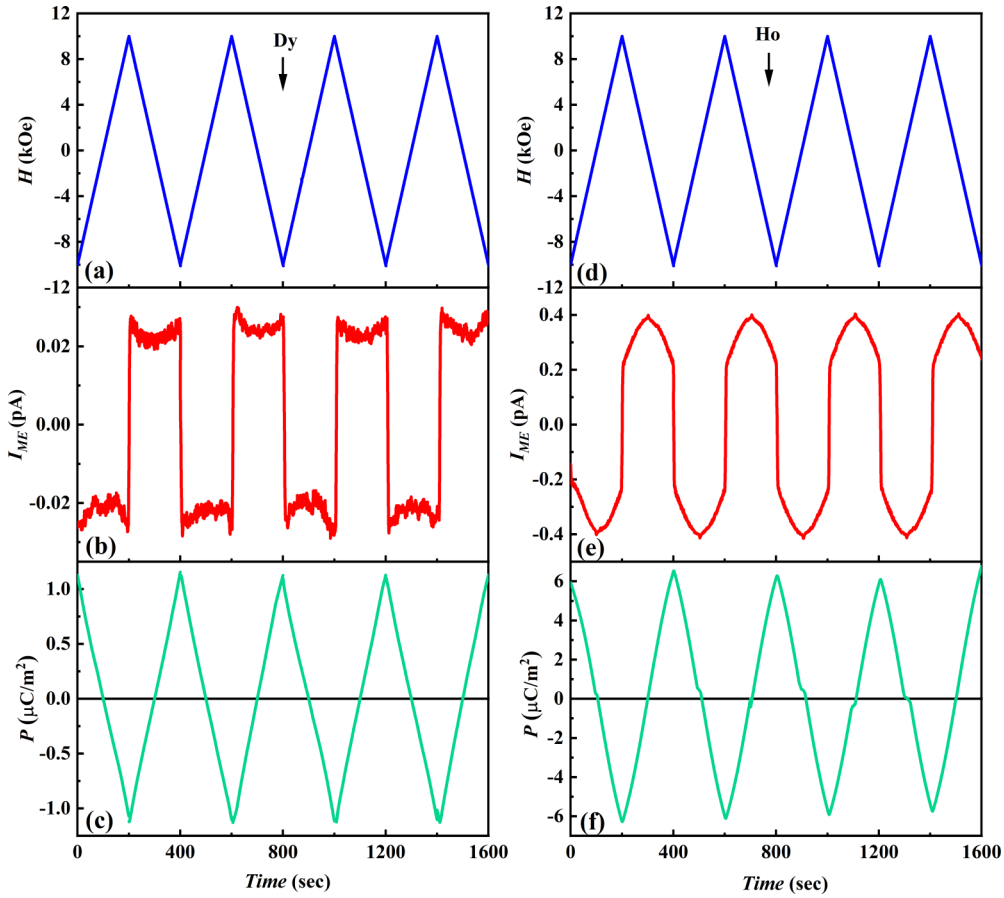

FIG. 6. Magnetoelectric current measured against the magnetic field for both compounds. Left panel: Dy_2BaCuO_5. Right panel: Ho_2BaCuO_5.

The monoclinic magnetic group $P112'_1/a$ [standard setting $P2'_1/c$, No. 14.77, 1D-$\mathbf{k}_{C2}$ *irreps*: mGM_4^-, and 2D-$\mathbf{k}_{C1}$ *irreps*: mY_1: (a, a)] gives a splitting into two sites for each one of the initial three sites (4*c*) in the paramagnetic state. This splitting has been previously observed from spectroscopic studies [36]. The number of magnetic free parameters for this group is $3 \times (3 + 3) = 18$. Nullifying the **b**-axis components (which are close to zero) of the magnetic moments corresponding to the contribution of the secondary mGM_3^- *irrep,* one obtains the 12 free parameters. We have performed a symmetry mode refinement in $P112'_1/a$ (primary order parameter constituted by the *irreps* mY_1 and mGM_4^-, secondary order parameter mGM_3^-) as described in the literature using the most recent version of FULLPROF [44,52]. The results of the refinement are given in Fig. S21 and Table SV in the Supplemental Material [44]. The contribution of the different *irreps* through the amplitude of the magnetic modes are explicit in the evolution of the magnetic structure of Ho_2BaCuO_5, which can be seen in Fig. S23(a) in the Supplemental Material [44]. To simplify the representation, in Fig. 10, we show the magnetic moments and their components, deduced from the values of the amplitudes of symmetry modes, as a function of temperature, for the case in which we consider that there is no contribution to the mGM_3^- *irrep* (moments along *b* are set to zero). The complete magnetic moments with the contribution of all modes are provided in the Supplemental Material [44]. Notice that the magnetic moment of Ho1, contrary to Ho2, in the region $T > 8$ K is relatively small; this is because the molecular field at the Ho2 site (surrounded by six Cu^{2+} ions) is higher than that of the Ho1 site (surrounded by three Cu^{2+} ions), like Dy_2BaCuO_5. The scheme of the magnetic structure with all magnetic free parameters can be seen in Fig. 9(b). The magnetic structure of Ho_2BaCuO_5 differs from that of Dy_2BaCuO_5 at low temperatures. The presence of the two propagation vectors in the former case and the strong reorientations of magnetic moments as a function of temperature make Ho_2BaCuO_5 possess a relatively labile magnetic

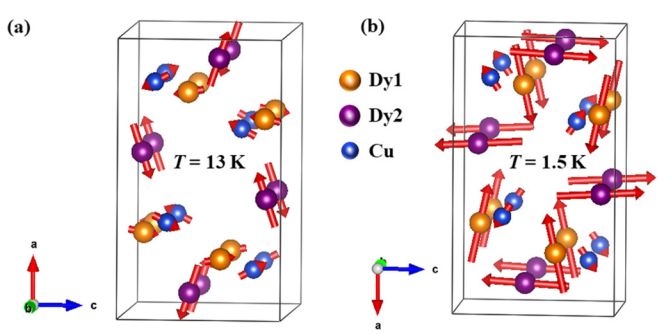

FIG. 7. Representation of magnetic structure of Dy_2BaCuO_5 at (a) 13 K and (b) 1.5 K (orange = Dy1, purple = Dy2, and blue = Cu). The magnetic moments of Dy1 and Cu atoms for 13 K and Cu for 1.5 K have been multiplied by 2 for display purposes.

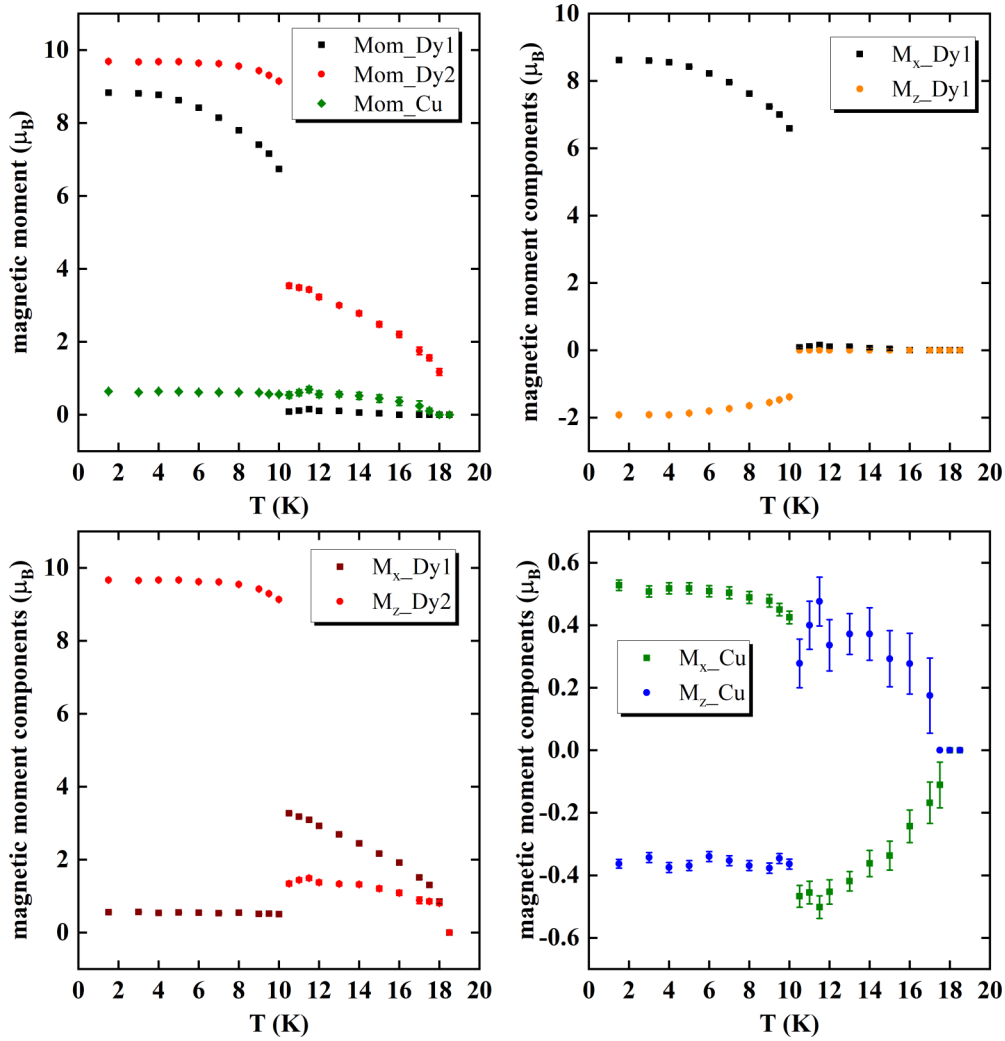

FIG. 8. The ordered magnetic moments and their components for Dy1, Dy2, and Cu as a function of temperature for Dy_2BaCuO_5.

structure sensitive to magnetic and thermal perturbations. As in the case of the Dy compound, the magnetic moments of Ho2 sites experience a drastic reorientation, making the coupling along the **b** axis ferromagnetic below T_N^R. The Ho1 site, which interacts weakly with the surrounding magnetic atoms, experiences the stronger changes with temperature.

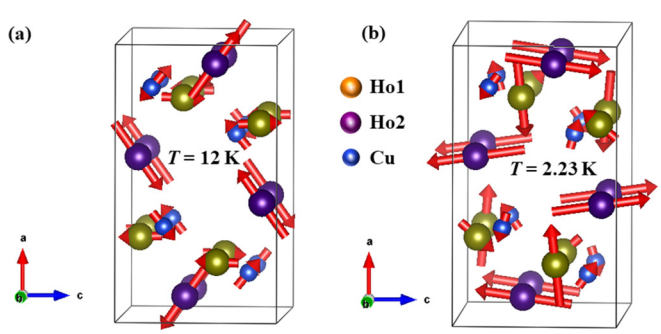

FIG. 9. Representation of the magnetic structures of Ho_2BaCuO_5 at (a) $T = 12.0$ K (WISH) and (b) 2.3 K (D1B). The magnetic moments of Ho1 and Cu atoms at 12 K and Cu at 2.3 K have been multiplied by 2 for display purposes.

The magnetic structures of Dy_2BaCuO_5 and Ho_2BaCuO_5 are unusual and complex. The presence of two magnetic sublattices formed by Cu^{2+} and R^{3+} ions and two different sites for the R^{3+} ions are responsible for this behavior. At T_N^{Cu}, spin ordering occurs with $\mathbf{k} = (0, \frac{1}{2}, 0)$ under the influence of the Cu-Cu exchange interaction through the path Cu^{2+}-O^{2-}-Dy^{3+}-O^{2-}-Cu^{2+} in both compounds. The Dy and Ho magnetic moments become weakly polarized by Cu^{2+} moments below T_N^{Cu}. Upon lowering the temperature, independent ordering of Dy and Ho spins occur with different **k**-vectors, as mentioned earlier. $R1$ magnetic moments point along the R-O bonds in both compounds due to a strong single-ion anisotropy together with isotropic and anisotropic exchanges [36]. However, theoretical calculations on crystal field splitting of R^{3+} ions and single-crystal study would help understand the role of anisotropy and the unusual magnetic structures of R_2BaCuO_5 (R = Dy and Ho).

Finally, below T_N^{Cu}, the P_b112_1/n spin structure preserves the inversion center in both compounds and does not allow a magnetoelectric effect due to the magnetic point group $2/m1'$, whereas below the T_N^R, the observed magnetic symmetry $Pnm'a$ (magnetic point group $mm'm$) for Dy and $P112_1'/a$ (magnetic point group $2'/m$) for Ho allow the linear

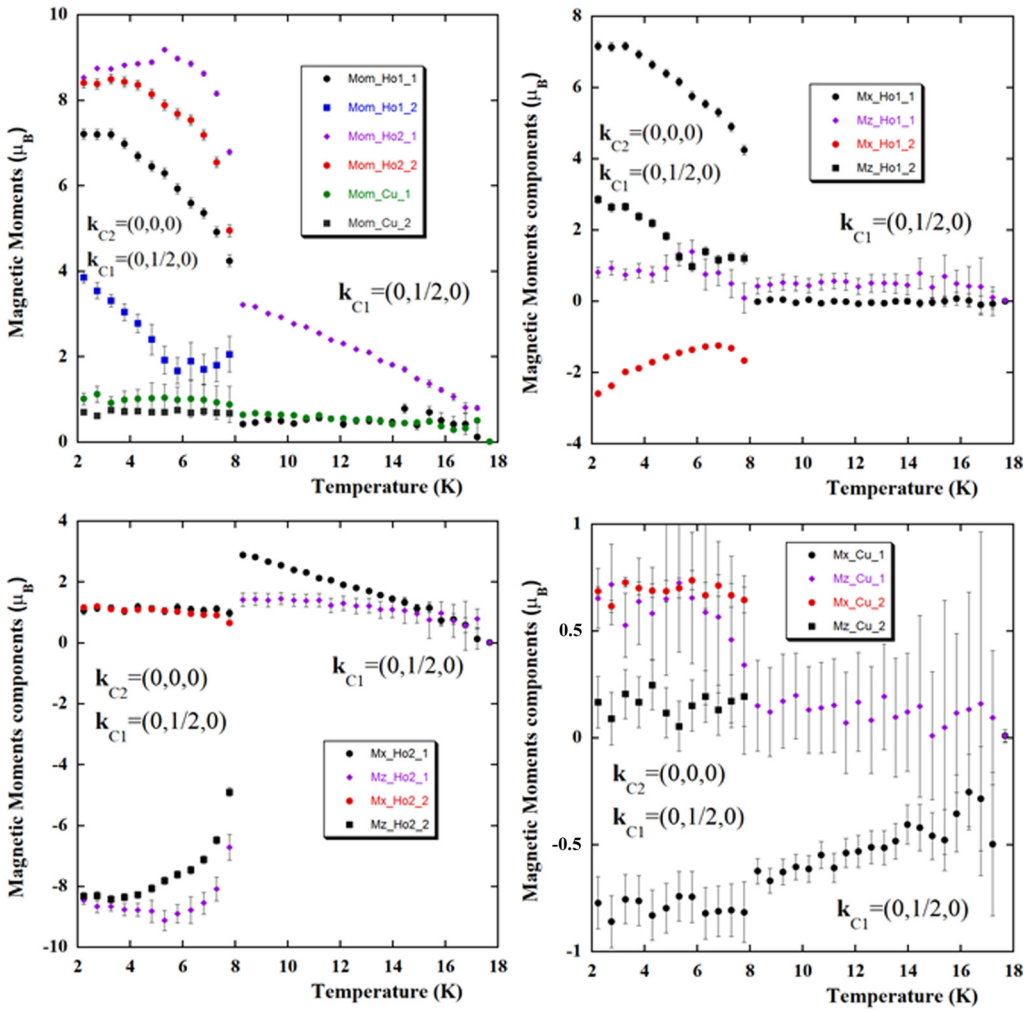

FIG. 10. Magnetic moments and their components for atoms Ho1, Ho2, and Cu as a function of temperature for Ho_2BaCuO_5. The refinements have been performed with no contribution of mGM_3^- (no y components). In the region of $\mathbf{k}_{C1}$ ($T > 8$ K), there are single sites (Ho1_1, Ho2_1, and Cu_1), and in the region of two propagation vectors $\mathbf{k}_{C1} + \mathbf{k}_{C2}$ ($T < 8$ K), the sites of magnetic atoms split into two inequivalent positions (Ho1_1, Ho1_2, Ho2_1, Ho2_2, Cu_1, Cu_2).

magnetoelectric effect [15]. The respective magnetoelectric tensors, in the standard setting, are given by [15]

$$\alpha = \begin{pmatrix} 0 & 0 & \alpha_{13} \\ 0 & 0 & 0 \\ \alpha_{31} & 0 & 0 \end{pmatrix} \text{ and } \begin{pmatrix} 0 & \alpha_{12} & 0 \\ \alpha_{21} & 0 & \alpha_{23} \\ 0 & \alpha_{32} & 0 \end{pmatrix}.$$

The presence of nonzero off-diagonal magnetoelectric coefficients allows the magnetoelectric terms corresponding to $P \perp H$ [47]. Indeed, this is confirmed by the large polarization in the $E \perp H$ configuration. The nonzero polarization observed in $E \parallel H$ is due to the polycrystalline nature of the samples. The presence of R ions with high spin-orbit interaction can introduce strong spin-lattice coupling in both compounds. Therefore, the observed magnetoelectric effect can be significantly large for these compounds. Moreover, the magnetic ions (Cu^{2+} and R^{3+}) are located on local noncentrosymmetric sites with the point group (m), and their spins predominantly lie in the **ac**-plane, as confirmed by the neutron diffraction. This implies that local electric dipole moments exist for all the magnetic ions lying in the **ac**-plane. Thus, magnetic symmetries in both cases allow the single-ion contributions to the magnetoelectric effect with large polarization due to rare-earth ions [38,42]. However, it requires theoretical work to understand the microscopic mechanism of the magnetoelectric effect.

In these compounds, there are no direct Cu-Cu, Cu-O-Cu, or Cu-O-O-Cu bonds. Thus, the possible magnetic exchange path is Cu-O-R-O-Cu. Due to this, the magnetic interactions between R and Cu ($4f$-$3d$ coupling) play a crucial role in green phase compounds. However, R ion magnetic anisotropy, crystal field effects, and the strength of the $4f$-$3d$ interaction decide the ordering of the R ion along with the Cu spins. In the green phase compounds, only Gd orders simultaneously with Cu because of the absence of crystal field effects due to the ground S-state term of Gd ion. However, from our neutron diffraction measurements, it was clear that the Dy and Ho spins are ordered below T_N^{Cu} due to induced moment by the Cu moments. The independent ordering of Dy and Ho spins at T_N^R induces reorientation of Cu spin moments and linear magnetoelectric effect. Also, the absence of R ion magnetic ordering in isostructural compounds R_2BaZnO_5 suggests the importance of the magnetic exchange path (Cu-O-R-O-Cu) in the green

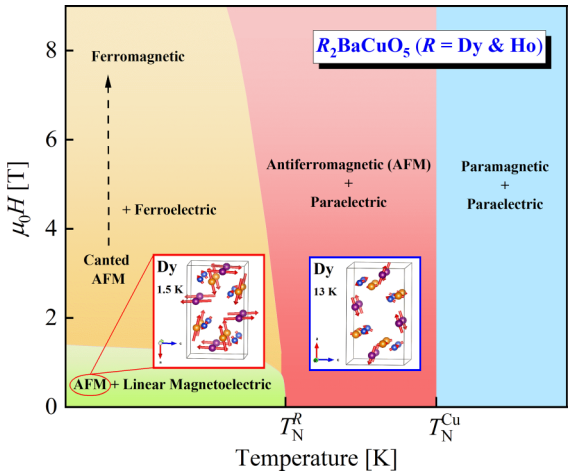

FIG. 11. Scheme of the H-T phase diagram for R_2BaCuO_5 (R = Dy and Ho) along with the magnetic structures of Dy_2BaCuO_5 in two phases are shown.

phase family [34]. Moreover, this behavior is different in Sm_2BaCuO_5 and Gd_2BaCuO_5, where linear magnetoelectric effect and multiferroicity are observed at Cu ordering temperature [4,38]. Therefore, we believe that the $4f$-$3d$ interaction plays a pivotal role in determining the magnetic structure and the associated magnetoelectric coupling in this family of compounds.

Under applied magnetic fields, both compounds exhibit field-induced metamagnetic transitions below T_N^R. Due to the remarkable magnetic anisotropy, applied magnetic fields can change the R sublattices spin structure and affect the Cu spin structure due to strong $4f$-$3d$ interaction, resulting in metamagnetic transitions. The resulting new spin states should be associated with nonlinear electric polarization with a magnetic field indicating the ferroelectric nature at high magnetic fields ($H > 1.2$ T). At fields ($\sim$7 T), though the polarization decreased, there is a finite ferroelectric polarization. This allows the control of the magnetization (polarization) by using an electric field (magnetic field) essential for the applications. From these results, we have illustrated the H-T phase diagram for R_2BaCuO_5 (R = Dy and Ho) in Fig. 11. Single-crystal neutron diffraction studies are required for a better understanding of the magnetoelectric coupling in these compounds.

IV. CONCLUSIONS

In conclusion, we have systematically investigated the linear magnetoelectric effect and field-induced ferromagnetism and ferroelectricity in the well-known green phase compounds R_2BaCuO_5 (R = Dy and Ho). Both exhibit long-range antiferromagnetic ordering of Cu^{2+} ($T_N^{Cu} = 18.5$ and 17.5 K) and R^{3+} ions ($T_N^{Dy} = 10.7$ K and $T_N^{Ho} = 8$ K) for Dy and Ho compounds, respectively. The applied magnetic field induces electric polarization at T_N^R, which varies linearly up to a critical field, confirming the linear magnetoelectric effect. The observed linear magnetoelectric effect is consistent with the magnetic symmetry. Under applied magnetic fields > 1.2 T, they show field-induced metamagnetic transitions with a large magnetization and ferroelectric polarization. The $4f$-$3d$ interaction plays a vital role in governing the magnetic structure and associated magnetoelectric properties. This paper opens a route to design multiferroic or magnetoelectric materials by tuning the f-d exchange interaction.

ACKNOWLEDGMENTS

The authors A.S. and P.Y. would like to acknowledge Sheikh Saqr Laboratory and International Centre for Materials Science at Jawaharlal Nehru Centre for Advanced Scientific Research for various experimental facilities. P.Y. acknowledges University Grants Commission for Ph.D. Fellowship (Award No. 2121450729). The authors acknowledge the Science and Technology Facility Council, U.K., for neutron beam time on the WISH diffractometer.

[1] T. Kimura, T. Goto, H. Shintani, K. Ishizaka, T. Arima, and Y. Tokura, Nature (London) **426**, 55 (2003).
[2] N. Hur, S. Park, P. A. Sharma, J. S. Ahn, S. Guha, and S. W. Cheong, Nature (London) **429**, 392 (2004).
[3] Y. Tokunaga, S. Iguchi, T. Arima, and Y. Tokura, Phys. Rev. Lett. **101**, 097205 (2008).
[4] P. Yanda, I. V. Golosovsky, I. Mirebeau, N. V. Ter-Oganessian, J. Rodríguez-Carvajal, and A. Sundaresan, Phys. Rev. Research **2**, 023271 (2020).
[5] P. Yanda, S. Mishra, and A. Sundaresan, Phys. Rev. Mater. **5**, 074406 (2021).
[6] W. Eerenstein, N. D. Mathur, and J. F. Scott, Nature (London) **442**, 759 (2006).
[7] M. Fiebig, J. Phys. D: Appl. Phys. **38**, R123 (2005).
[8] D. Khomskii, Physics **2**, 20 (2009).
[9] S. W. Cheong and M. Mostovoy, Nat. Mater. **6**, 13 (2007).
[10] J. F. Scott, J. Mater. Chem. **22**, 4567 (2012).
[11] S. Fusil, V. Garcia, A. Barthélémy, and M. Bibes, Annu. Rev. Mater. Res. **44**, 91 (2014).
[12] J. P. Rivera, Eur. Phys. J. B **71**, 299 (2009).
[13] I. E. Dzyaloshinskii, Sov. Phys. JETP **10**, 628 (1960).
[14] D. N. Astrov, Sov. Phys. JETP **11**, 708 (1960).
[15] R. E. Newnham, *Properties of Materials: Anisotropy, Symmetry, Structure* (Oxford University Press, Oxford, 2005).
[16] N. A. Hill, J. Phys. Chem. B **104**, 6694 (2000).
[17] J. Wang, J. B. Neaton, H. Zheng, V. Nagarajan, S. B. Ogale, B. Liu, D. Viehland, V. Vaithyanathan, D. G. Schlom, and U. V. Waghmare, Science **299**, 1719 (2003).
[18] J. Hwang, E. S. Choi, H. D. Zhou, J. Lu, and P. Schlottmann, Phys. Rev. B **85**, 024415 (2012).
[19] N. Mufti, G. R. Blake, M. Mostovoy, S. Riyadi, A. A. Nugroho, and T. T. M. Palstra, Phys. Rev. B. **83**, 104416 (2011).
[20] Y. Fang, L. Y. Wang, Y. Q. Song, T. Tang, D. H. Wang, and Y. W. Du, Appl. Phys. Lett. **104**, 132908 (2014).
[21] E. Fischer, G. Gorodetsky, and R. M. Hornreich, Solid State Commun. **10**, 1127 (1972).
[22] Y. Fang, W. P. Zhou, S. M. Yan, R. Bai, Z. H. Qian, Q. Y. Xu, D. H. Wang, and Y. W. Du, J. Appl. Phys. **117**, 17B712 (2015).

[23] Y. Fang, Y. Q. Song, W. P. Zhou, R. Zhao, R. J. Tang, H. Yang, L. Y. Lv, S. G. Yang, D. H. Wang, and Y. W. Du, Sci. Rep. **4**, 3860 (2014).
[24] A. Maignan and C. Martin, Phys. Rev. B **97**, 161106 (2018).
[25] R. Saha, S. Ghara, E. Suard, D. H. Jang, K. H. Kim, N. V. Ter-Oganessian, and A. Sundaresan, Phys. Rev. B **94**, 014428 (2016).
[26] S. Ghara, N. V. Ter-Oganessian, and A. Sundaresan, Phys. Rev. B **95**, 094404 (2017).
[27] S. Mishra, P. Yanda, and A. Sundaresan, Phys. Rev. B **103**, 214443 (2021).
[28] Y. Tokunaga, N. Furukawa, H. Sakai, Y. Taguchi, T. Arima, and Y. Tokura, Nat. Mater. **8**, 558 (2009).
[29] X. Shen, L. Zhou, Y. Chai, Y. Wu, Z. Liu, Y. Yin, H. Cao, C. Dela Cruz, Y. Sun, C. Jin, A. Muñoz, J. A. Alonso, and Y. Long, NPG Asia Mater. **11**, 50 (2019).
[30] C. Michel and B. Raveau, J. Solid State Chem. **43**, 73 (1982).
[31] R. Z. Levitin, B. V. Mill, V. V. Moshchalkov, N. A. Samarin, V. V. Snegirev, and J. Zoubkova, J. Magn. Magn. Mater. **90**, 536 (1990).
[32] V. V. Moshchalkov, N. A. Samarin, I. O. Grishchenko, B. V. Mill, and J. Zoubkova, Solid State Commun. **78**, 879 (1991).
[33] I. V. Paukov, M. N. Popova, and B. V. Mill, Phys. Lett. A **169**, 301 (1992).
[34] G. F. Goya, R. C. Mercader, M. T. Causa, and M. Tovar, J. Phys. Condens. Matter **8**, 8607 (1996).
[35] R. Z. Levitin, B. V. Mill, V. V. Moshchalkov, N. A. Samarin, V. V. Snegirev, and Y. Zoubkova, Solid State Commun. **73**, 443 (1990).
[36] M. Baran, H. Szymczak, S. A. Klimin, M. N. Popova, and R. Z. Levitin, J. Exp. Theor. Phys. **84**, 175 (1997).
[37] A. Indra, S. Mukherjee, S. Majumdar, O. Gutowski, M. v. Zimmermann, and S. Giri, Phys. Rev. B **100**, 014413 (2019).
[38] P. Yanda, N. V. Ter-Oganessian, and A. Sundaresan, Phys. Rev. B **100**, 104417 (2019).
[39] I. V. Golosovsky, V. P. Plakhtii, V. P. Kharchenkov, J. Zoubkova, B. V. Mill, M. Bonnet, and E. Roudeau, Fiz. Tve. Tela **34**, 1483 (1992).
[40] I. V. Golosovsky, P. Böni, and P. Fischer, Solid State Commun. **87**, 1035 (1993).
[41] A. K. Ovsyanikov, I. V. Golosovsky, I. A. Zobkalo, and I. Mirebeau, J. Magn. Magn. Mater. **353**, 71 (2014).
[42] V. P. Sakhnenko and N. V. Ter-Oganessian, J. Phys.: Condens. Matter **24**, 266002 (2012).
[43] L. C. Chapon, P. Manuel, P. G. Radaelli, C. Benson, L. Perrott, S. Ansell, N. J. Rhodes, D. Raspino, D. Duxbury, and E. Spill, Neutron News **22**, 22 (2011).
[44] See Supplemental Material at http://link.aps.org/supplemental/10.1103/PhysRevB.104.144401 for x-ray and neutron diffraction, crystal and magnetic structure refinements, Curie fit, derivative of magnetization, dielectric, pyroelectric, and magnetoelectric measurements and MCIF files for the magnetic structures of Dy_2BaCuO_5 and Ho_2BaCuO_5 which can be visualized by using VESTA software.
[45] A. Salinas-Sanchez, J. L. Garcia-Muñoz, J. Rodriguez-Carvajal, R. Saez-Puche, and J. L. Martinez, J. Solid State Chem. **100**, 201 (1992).
[46] C. De, S. Ghara, and A. Sundaresan, Solid State Commun. **205**, 61 (2015).
[47] S. Shtrikman and D. Treves, Phys. Rev. **130**, 986 (1963).
[48] J. Rodriguez-Carvajal, Fullprof: A program for Rietveld refinement and pattern matching analysis, in *Abstract of the Satellite Meeting on Powder Diffraction of the XV Congress of the IUCr*, Toulouse, France (1990), p. 127; Physica B **192**, 55 (1993); The fullprof suite can be freely downloaded from: https://www.ill.eu/sites/fullprof.
[49] B. J. Campbell, H. T. Stokes, D. E. Tanner, and D. M. Hatch, J. Appl. Crystallogr. **39**, 607 (2006).
[50] J. González-Platas, N. A. Katcho, and J. Rodríguez-Carvajal, J. Appl. Cryst. **54**, 338 (2021).
[51] J. Rodríguez-Carvajal and F. Bourée, EPJ Web Conf. **22**, 00010 (2012).
[52] S. Ghara, E. Suard, F. Fauth, T. T. Tran, P. S. Halasyamani, A. Iyo, J. Rodríguez-Carvajal, and A. Sundaresan, Phys. Rev. B **95**, 224416 (2017).